



HAL
open science

Thermal energy transport in a surface phonon-polariton crystal

Jose Ordonez-Miranda, Laurent Tranchant, Younes Ezzahri, Jérémie Drevillon, Karl Joulain, Sebastian Volz

► **To cite this version:**

Jose Ordonez-Miranda, Laurent Tranchant, Younes Ezzahri, Jérémie Drevillon, Karl Joulain, et al.. Thermal energy transport in a surface phonon-polariton crystal. *Physical Review B: Condensed Matter and Materials Physics (1998-2015)*, 2016, 93, pp.3. 10.1103/physrevb.93.035428 . hal-01336738

HAL Id: hal-01336738

<https://centralesupelec.hal.science/hal-01336738v1>

Submitted on 23 Sep 2024

HAL is a multi-disciplinary open access archive for the deposit and dissemination of scientific research documents, whether they are published or not. The documents may come from teaching and research institutions in France or abroad, or from public or private research centers.

L'archive ouverte pluridisciplinaire **HAL**, est destinée au dépôt et à la diffusion de documents scientifiques de niveau recherche, publiés ou non, émanant des établissements d'enseignement et de recherche français ou étrangers, des laboratoires publics ou privés.

Thermal Energy Transport in a Surface Phonon-Polariton Crystal


Jose Ordonez-Miranda,^{1,2} Laurent Tranchant,³ Karl Joulain,¹
Younes Ezzahri,¹ Jérémie Drevillon,¹ and Sebastian Volz²

¹*Institut Pprime, CNRS, Université de Poitiers-ENSMA, 2 Rue Pierre Brousse,
Bâtiment B25, TSA 41105,86073 Poitiers Cedex 9, France*

²*Laboratoire EM2C, CNRS, CentraleSupélec, Université Paris-Saclay,
Grande Voie des Vignes, 92295 Châtenay-Malabry cedex, France**

³*Department of Mechanical and Control Engineering, Kyushu Institute of Technology,
1-1 Sensui-cho, Tobata-ku, Kitakyushu 804-8550, Japan*

(Dated: January 9, 2016)

We demonstrate that the energy transport of surface phonon-polaritons can efficiently be observed in a crystal made up of a three-dimensional assembly of spheroidal nanoparticles of silicon carbide. The ultralow phonon thermal conductivity of this nanostructure along with its high surface area-to-volume ratio allows the predominance of the polariton energy over that generated by phonons. The polariton dispersion relation, propagation length, and thermal conductance are numerically determined as functions of the size, shape, and temperature of the nanoparticles. It is shown that the thermal conductance of a crystal with prolate nanoparticles at 500 K and a minor (major) axis of 50 nm ($5\ \mu\text{m}$) is $0.5\ \text{nW}\cdot\text{K}^{-1}$, which is comparable to the quantum of thermal conductance of polar nanowires. We also show that a nanoparticle size dispersion up to 200 nm, does not change significantly the polariton energy, which supports the technological feasibility of the proposed crystal.

PACS numbers: 65.60.+a; 65.80.-g; 65.90.+i

I. INTRODUCTION

Surface phonon-polaritons (SPhPs) are coupled states of optical phonons and electromagnetic waves that can significantly enhance the thermal energy transport along the interface of polar nanomaterials [1–4]. Theoretical [5–7] and experimental [8, 9] studies have shown that the propagation length of SPhPs can be more than three orders of magnitude larger than the phonon mean free path, which is of a few nanometers upward, for a wide variety of materials at room temperature [10, 11]. This sizeable difference on the mean free path of phonons and SPhPs yields a SPhP thermal conductivity of nanofilms [5, 7, 12] and a SPhP thermal conductance of nanowires [13] that could be comparable to the corresponding ones of phonons [14–21].

SPhP energy transport is determined by the permittivity and geometry of the involved polar nanomaterials and hence it can be modified by material discontinuities. Given that SPhPs are electromagnetic waves that propagate along the material interface, their energy transport is expected to increase as the material size is scaled down to nanoscales, due to the strengthening of the surface effects. This is the case of the SPhP thermal conductivity of nanofilms, which increases with the inverse third power of the film thickness mainly [6, 7]. The SPhP thermal conductivity of a 40-nm-thick thin film of silicon dioxide at 500 K and suspended in air is $4\ \text{W}\cdot\text{m}^{-1}\cdot\text{K}^{-1}$ [5, 12], which is more than twice the corresponding phonon counterpart. Higher values are found for thinner films and

higher temperatures. In a nanowire, on the other hand, SPhPs propagates ballistically and their contribution to the its thermal conductance is quantized and given by $\pi^2 k_B^2 T/3h$ [13], which is comparable to the phonon contribution, at low temperature [14, 15]. This comparability between the phonon and SPhP thermal conductivities and thermal conductances makes difficult to experimentally observe the SPhP energy transport. A nanostructure able to support the SPhP propagation and quench the phonon heat conduction is therefore desirable.

The purpose of this work is to theoretically demonstrate that the SPhP energy transport can efficiently be observed in a three-dimensional (3D) crystal made up of spheroidal polar nanoparticles. This is done by determining the SPhP thermal conductance of the proposed crystal and showing that its values can be as high as those of the quantum of thermal conductance of polar nanowires. The effects of the nanoparticle size, shape, and temperature are analyzed in detail.

II. SPhP ENERGY TRANSPORT

Let us consider a 3D assembly of polar nanoparticles in contact, as shown in Fig. 1(a). The nanoparticles are spheroids with semiaxis lengths along the x , y , and z axes of b , a , and a , respectively (Fig. 1(b)). The thermal energy transport along this nanoparticle crystal is expected to be dominated by SPhPs due to two main reasons: First, the relatively small nanoparticles along with their multiple interfaces act as thermal barriers that diminish remarkably the phonon heat conduction [22]. Second, the high surface area-to-volume ratio of the nanoparti-

* jose.ordonez@univ-poitiers.fr

cles favors the propagation of SPhPs along their surfaces. This crystal can be fabricated by the well-established micro/nanofabrication technique of focused ion beam direct writing, which has a relatively low deposition rate (normally, $0.05 \mu\text{m}^3/\text{s}$), but a comparatively high resolution of 80 nm [23]. Two other alternative techniques of fabrication are the 3D printing and the high-resolution stereolithography [24], which have been recently applied to fabricate 3D phononic crystals used for tailoring the phonon thermal conductivity [25, 26].

To quantify the energy transport of SPhPs propagating in the nanoparticle crystal shown in Fig. 1(a), we put it in thermal contact with two thermal baths set at the temperatures T_1 and T_2 ($T_1 > T_2$), as shown in Fig. 1(c). Under this thermal excitation, the polar molecules of the nanoparticles emit an electric field, as a result of their oscillating electrical dipoles. This field induces the excitation of neighboring electrical dipoles, which keep the propagation of the field (SPhP) along the z axis. Assuming that the thermal contacts between the thermal baths and the crystal are good enough [13] to allow the transmission of SPhPs from the left thermal bath to the right one, the SPhP propagation length Λ will be longer than the crystal length along the z axis and the thermal bath will exchange a net heat flux. Under this condition and taking into account that SPhPs follow the Bose-Einstein statistics [5], the net heat flux q of SPhPs propagating with speed V is given by [27]

$$q = \frac{1}{4\pi} \int \hbar\omega V \cos(\theta) [f(T_1) - f(T_2)] D(\omega) d\omega d\Omega, \quad (1)$$

where $2\pi\hbar$ is the Planck's constant, ω is the excitation frequency, $f(T) = [\exp(\hbar\omega/k_B T) - 1]^{-1}$ is the Bose-Einstein distribution function, $D(\omega) = \beta_R^2(\omega)/(2\pi^2 V)$ is the 3D density of SPhP states, β_R being the SPhP wave vector along the heat flux direction ($+z$ axis), and $d\Omega = \sin(\theta)d\theta d\phi$ is a differential of solid angle in spherical coordinates, with θ the angle between the SPhP velocity and heat flux. Equation (1) represents an extension of the Landauer formula [17, 28–30] for 3D heat transport. Considering that the difference of temperature $\Delta T = T_1 - T_2 \ll T = (T_1 + T_2)/2$, the change of distribution functions in Eq. (1) reduces to $f(T_1) - f(T_2) = \Delta T \partial f(T)/\partial T$. After performing the angular integration in Eq. (1), the thermal conductance $G = qS/\Delta T$ of the SPhP crystal can be expressed as

$$G = \frac{S}{8\pi^2} \int_{\omega_{\min}}^{\omega_{\max}} \hbar\omega\beta_R^2 \frac{\partial f(T)}{\partial T} d\omega. \quad (2)$$

where $S = \pi ab$ is the nanoparticle cross-section area "seen" by the SPhPs propagating along the z axis and ω_{\min} and ω_{\max} stand for the lowest and highest frequencies allowing their propagation. Equation (2) shows that G increases with the SPhP wave vector β_R , which depends on the material properties and geometry of the nanoparticles. The comparison of the thermal conductance in Eq. (2) with that for a linear chain of nanoparticles [31, 32], indicates that the 3D effect on G is taken into

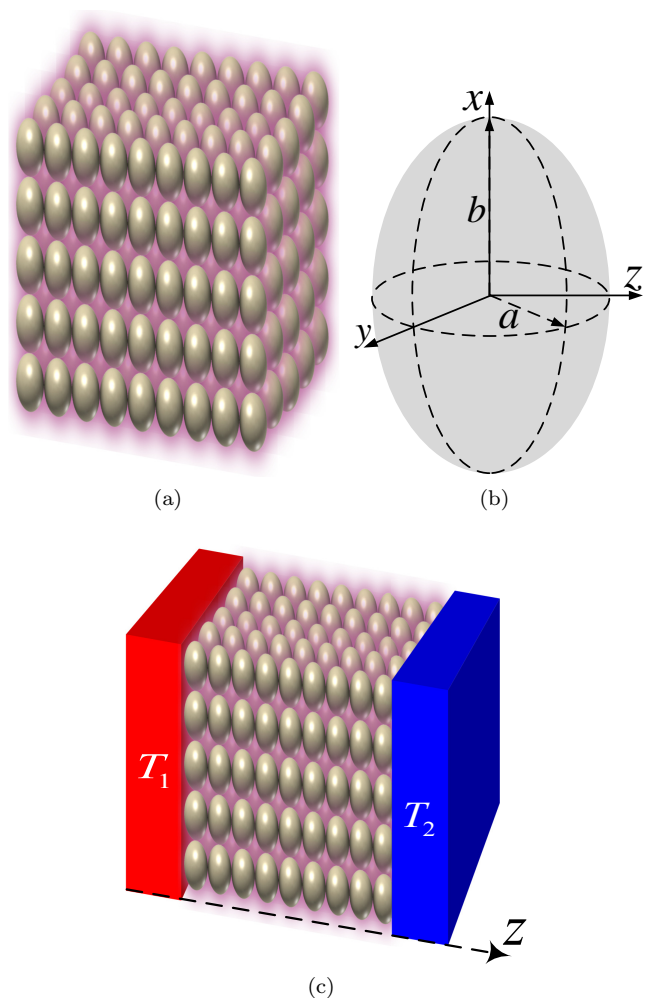


FIG. 1: (a) Surface phonon-polariton crystal made up of (b) spheroidal polar nanoparticles. (c) Heat transport along the SPhP crystal excited by two thermal baths. The purple glow around the nanoparticles represents the coupled electromagnetic field induced by their surface polarization.

account by means of the non-dimensional factor $S\beta_R^2/4\pi$, which is associated with the confinement of SPhPs to the nanoparticle surfaces [31]. Thus, Eq. (2) physically establishes that the stronger the confinement, the higher the energy transport of SPhPs, as expected.

The wave vector $\beta_R = \text{Re}(\beta)$ is determined by the dispersion relation of the SPhPs propagating along the z axis of the nanoparticle crystal shown in Fig. 1(a). The polar nanoparticles have a relative permittivity ϵ_1 and are embedded in a dielectric medium of relative permittivity ϵ_2 . Both media are assumed to be non-magnetic ($\mu_1 = \mu_2 = 1$) and that the electrical dipoles inside the nanoparticles are aligned parallel to the z axis, as established by the thermal excitation of the thermal baths shown in Fig. 1(c). In view of this alignment, the dipole-dipole interactions occur along the z axis mainly, and therefore the SPhP propagation in the 3D crystal can be

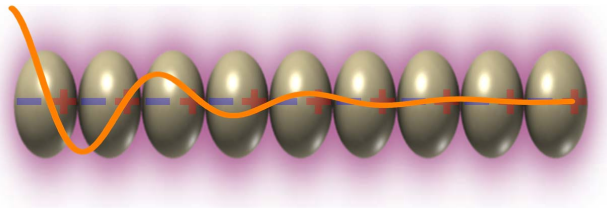


FIG. 2: Chain of spheroidal polar nanoparticles supporting the propagation of SPhPs due to the dipole-dipole interactions. The continuous line stands for the decay of SPhP electromagnetic field as it propagates along the chain.

modelled as that along a single chain of nanoparticles, as shown in Fig. 2. By solving the Maxwell equations under proper boundary conditions required for the existence of SPhPs [1, 5] along a chain of nanoparticles with longitudinal polarization, the following dispersion relation for the complex wave vector β is obtained [31]

$$-i + \alpha_e^{-1} = \frac{3}{X^3} [f_3(K, X) - iXf_2(K, X)], \quad (3)$$

where $X = 2ak_2$, $K = \beta/k_2$, $f_j(K, X) = Li_j(e^{iX(1+K)}) + Li_j(e^{iX(1-K)})$, and $Li_j(z) = \sum_{n=1}^{\infty} z^n/n^j$ is the polylogarithm function of order $j = 2, 3$ [33]. The wave vector $k_2 = \sqrt{\epsilon_2}\omega/c$ and normalized polarizability $\alpha_e = \alpha_s k_2^3/(6\pi\epsilon_2)$, ω being the excitation frequency, c the speed of light in vacuum, and α_s the electrostatic polarizability of the nanoparticles, which depends on their permittivity ϵ_1 and geometry [31]. The absorption of energy by the polar nanomaterials is accounted for their complex permittivity ϵ_1 , which turns α_e and $K = K_R + iK_I$, into complex parameters as well. The real ($K_R > 0$) and imaginary ($K_I > 0$) parts of the normalized wave vector K are associated with the propagation (along the $+z$ direction) and attenuation factor, respectively. For the case of interest, in which the SPhP propagation length $\Lambda = (2k_2K_I)^{-1}$ [12] is much larger than the center-to-center distance between the nanoparticles ($\Lambda \gg 2a$), the condition $K_I X \ll 1$ is fulfilled and the linear approximation of the Taylor series expansion of Eq.(3) in powers of $K_I X$ allows the decoupling of its real and imaginary parts to yield

$$\text{Re}(\alpha_e^{-1}) = \frac{3}{X^3} [g_3^+(K_R, X) + Xg_2^+(K_R, X)], \quad (4a)$$

$$K_I = -\frac{X^2}{3} \frac{\text{Im}(\alpha_e^{-1})}{g_2^-(K_R, X) - Xg_1^-(K_R, X)}, \quad (4b)$$

where the functions g_j^\pm are independent of K_I and given by

$$g_j^\pm(K_R, X) = Cl_j[X(1+K_R)] \pm Cl_j[X(1-K_R)], \quad (5)$$

$Cl_j(\theta)$ being the real-valued Clausens functions of order $j = 1, 2, 3$ [33, 34]. For low frequencies and/or small

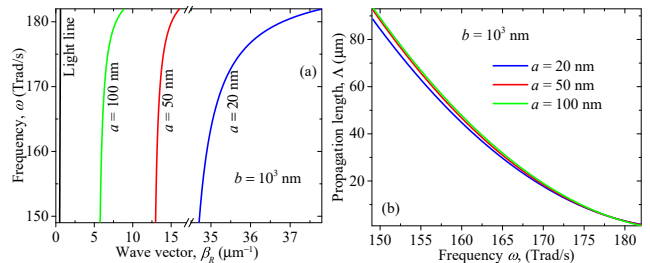


FIG. 3: (a) Dispersion relation and (b) propagation length of SPhPs as a function of frequency, for SPhP crystals with different shapes of SiC nanoparticles surrounded by air.

interparticle distances, such that $X \ll 1$, the contribution of g_2^+ disappears and the SPhP propagation is therefore driven by g_3^+ mainly. Equation (4b) allows us to determine K_I and therefore the SPhP propagation length $\Lambda = (2k_2K_I)^{-1}$, after solving numerically Eq. (4a) for $K_R = \beta_R/k_2$. In absence of energy absorption ($\text{Im}(\alpha_e^{-1}) = 0$), $K_I = 0$ and Eq. (4a) reduces to the previous one [34], derived for ideal lossless nanoparticles.

The obtained dispersion relation and propagation length are now numerically quantified for SPhP crystals with SiC nanoparticles surrounded by air, which is transparent ($\epsilon_2 = 1$) within the range of frequencies where the SiC supports the SPhP propagation. The permittivity ϵ_1 of the crystalline SiC at room temperature is well described by the damped harmonic oscillator model [5, 35]

$$\epsilon_1(\omega) = \epsilon_\infty \left(1 + \frac{\omega_L^2 - \omega_T^2}{\omega_T^2 - \omega^2 - i\Gamma\omega} \right), \quad (6)$$

where $\omega_L = 182$ Trad/s and $\omega_T = 149$ Trad/s are the longitudinal and transversal optical frequencies, respectively; $\Gamma = 0.892$ Trad/s is a damping constant and $\epsilon_\infty = 6.7$ is the high frequency permittivity [36]. The maximum of the imaginary part of ϵ_1 occurs at $\omega = \omega_T$, which indicates that SiC absorbs more energy from the SPhPs at this frequency. Furthermore, the real part $\text{Re}(\epsilon_1)$ takes negative values within the frequency interval $\omega_T < \omega < \omega_L$, which renders the main contribution to the propagation and energy transport of SPhPs [5], as shown below. These values of the permittivity are expected to be valid for nanoparticle sizes larger than 5 nm [37] and temperature lower than 600 K [38].

III. RESULTS AND DISCUSSIONS

The dispersion relation and propagation length of SPhPs traveling along the nanoparticles/air interface of the SPhP crystal are shown in Figs. 3(a) and 3(b), respectively. At low frequency, the SPhP wave vector β_R tends to be parallel to the light line ($\beta_R = k_2$), which shows the photon-like nature of the SPhPs. As the frequency increases, β_R takes larger values and separates

from the light line, what enhances the confinement of the SPhPs to the nanoparticle surface [31] and their energy transport, as established by Eq. (2). The major contribution to the SPhP thermal conductance arises therefore from the high frequency regime. This confinement strengthens as the nanoparticle radius a reduces, due to the stronger surface dipole interactions as the aspect ratio b/a of the nanoparticles increases. However, the increase of β_R comes along with the reduction of the SPhP propagation length Λ , as shown in Fig. 3(b). The trade-off between β_R and Λ indicates that the excitation frequencies of SPhPs should be high enough to enhance their confinement and energy transport, but low enough not to significantly reduce their propagation length. For the three nanoparticle radii a under consideration, Λ is almost independent of a , within all the frequency range of SPhP propagation. This is due to the large aspect ratio of the nanoparticles ($b/a \geq 10$), for which the propagation length $\Lambda = (b/6) (Xg_1^- - g_2^-) \text{Im}[(\epsilon_1 - \epsilon_2) / (\epsilon_1 + \epsilon_2)]$ (see Eq. (4b)) becomes weakly dependent on a and reaches its longest asymptotic values. Shorter propagation lengths are obtained for smaller aspect ratios, what indicates that cylindrical nanoparticles with high aspect ratios ($b/a > 10$) are able to maximize the propagation distance of SPhPs as well as to enhance their confinement (Fig. 3(a)). For SPhPs propagating with a frequency $\omega = 150$ Trad/s along nanoparticles with $(a, b) = (50, 1000)$ nm, their propagation length is $90 \mu\text{m}$ (900 nanoparticles). This distance represents the maximum size of the SPhP crystal along its z axis (Fig.1(c)), to ensure the exchange of thermal energy between the thermal baths. Furthermore, Figs. 4(a) and 4(b) show that when the vertical radius of the nanoparticles increases from $b = 900$ nm to $b = 1100$ nm, neither the dispersion relation nor the propagation length are significantly modified. This is reasonable due to the fact that the SPhP propagation is mainly driven by the dipole interactions along the z axis, and hence by the nanoparticle radius a . Therefore, a 200 nm-dispersion on b , which is expected to be present in real crystals, does not change remarkably the SPhP energy of the crystal (Eq. (2)). Greater size dispersions or the presence of other imperfections can remarkably weaken the dipole interactions and consequently the energy transport of polaritons. Fortunately, the resolution of the focused ion beam direct writing technique is 80 nm [23] and hence the fabrication of the proposed 3D crystal with the required regular (not perfect) arrangement of particles is feasible.

Figures 5(a) and 5(b) show the SPhP thermal conductance G of the crystal as a function of the nanoparticle radius a and temperature T , respectively. Note that G increases as a reduces, due to the increasing SPhP confinement shown by the dispersion relation in Fig. 3(a). This enhancement of G is strengthened by the temperature rise of the crystal, especially from 300 K to 500 K. When a is scaled down from 200 nm to 20 nm, G increases by more than one order of magnitude, which points out that long cylindrical nanoparticles are the suitable candidates

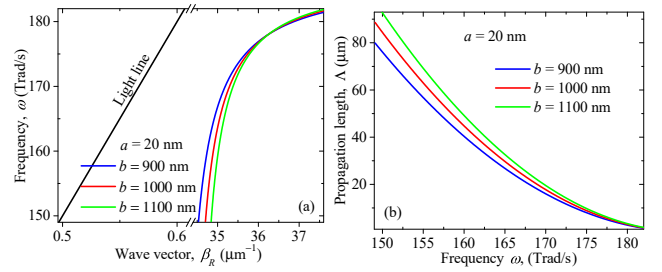


FIG. 4: Frequency dependence of the (a) Dispersion relation and (b) propagation length of SPhPs, for crystals with different shapes of SiC nanoparticles surrounded by air.

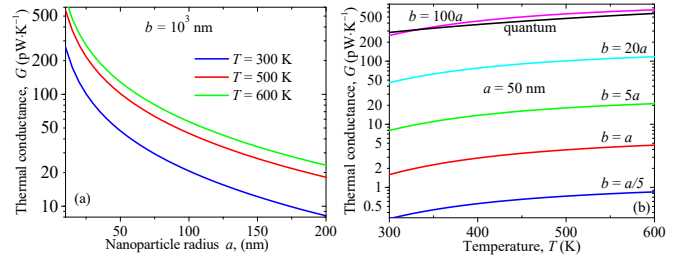


FIG. 5: Thermal conductance of the SPhP crystal made up of spheroidal SiC nanoparticles, as a function of their (a) horizontal radius and (b) temperature. The quantum of thermal conductance is given by $G_0 = \pi^2 k_B^2 T / 3h$ [13].

to observe a sizeable energy transport by SPhPs. This is confirmed in Fig. 5(b), which shows that the SPhP thermal conductance of a crystal with spherical ($b = a$) and oblate ($b = a/5$) nanoparticles is much smaller than that for oblate (cylindrical) ones. The longer the aspect ratio b/a , the higher the thermal conductance. For $(b, a) = (5000, 50)$ nm, G is comparable to the quantum of thermal conductance, which shows that the proposed SPhP crystal can be as good polariton conductor as a polar nanowire. However, the advantage of this crystal is its ultralow phonon heat conduction, which can facilitate the observation of the SPhP heat transport.

The SPhP thermal conductance of the crystal could be measured generating SPhPs by thermal excitation at one surface of the crystal, and detecting their diffraction at the opposite parallel surface. This diffracted signal contains information about the SPhP heat flux and can be recorded through an IR microscope, over a wide range of frequencies and temperatures comparable to room temperature. Given that the phonon energy contribution is negligible, the experimental data are expected to yield a SPhP thermal conductance with a quasi linear dependence on temperature (Fig. 5(b)), which is the signature of the SPhP energy transport in the nanoparticle crystal.

IV. CONCLUSIONS

The thermal conductance due to the propagation of surface phonon-polaritons in a 3D crystal made up of spheroidal SiC nanoparticles has been determined and shown to be comparable to the quantum of thermal conductance of polar nanowires, within a wide range of temperature. This relatively high thermal conductance along

with the ultralow phonon counterpart demonstrates that the energy transport of these polaritons could be unambiguously observed in a polariton crystal with cylindrical nanoparticles. Furthermore, it has been shown that the slight size dispersion of the nanoparticles, along the direction perpendicular to the propagation one, does not change significantly the polariton energy, which supports the technological viability of the proposed approach.

-
- [1] V. M. Agranovich and D. L. Mills, *Electromagnetic Waves at Surfaces and Interfaces* (North-Holland Pub. Co., Minesota, 1982).
- [2] A. I. Volokitin and B. N. J. Persson, *Rev. Mod. Phys.* **79**, 1291 (2007).
- [3] F. Yang, J. R. Sambles, and G. W. Bradberry, *Phys. Rev. B* **44**, 5855 (1991).
- [4] M. Li, P. Lewin, A. V. Kretinin, J. D. Caldwell, K. S. Novoselov, T. Taniguchi, K. Watanabe, F. Gaussmann, and T. Taubner, *Nature Commun.* **6**, 7507 (2015).
- [5] D.-Z. A. Chen, A. Narayanaswamy, and G. Chen, *Phys. Rev. B* **72**, 155435 (2005).
- [6] J. Ordonez-Miranda, L. Tranchant, T. Antoni, Y. Chalopin, and S. Volz, *J. Appl. Phys.* **115**, 054311 (2014).
- [7] J. Ordonez-Miranda, L. Tranchant, B. Kim, Y. Chalopin, T. Antoni, and S. Volz, *Appl. Phys. Express* **7**, 035201 (2014).
- [8] P. Lambin, J. Vigneron, A. Lucas, P. Thiry, M. Liehr, J. Pireaux, R. Caudano, and T. Kuech, *Phys. Rev. Lett.* **56**, 1842 (1986).
- [9] D. Z. A. Chen and G. Chen, *Appl. Phys. Lett.* **91**, 121906 (2007).
- [10] M. Kanskar and M. N. Wybourne, *Phys. Rev. B* **50**, 168 (1994).
- [11] N. Stojanovic, D. H. S. Maithripala, J. M. Berg, and M. Holtz, *Phys. Rev. B* **82**, 075418 (2010).
- [12] J. Ordonez-Miranda and et al., *J. App. Phys.* **113**, 084311 (2013).
- [13] J. Ordonez-Miranda, L. Tranchant, B. Kim, Y. Chalopin, T. Antoni, and S. Volz, *Phys. Rev. Lett.* **112**, 055901 (2014).
- [14] B. A. Glavin, *Phys. Rev. Lett.* **86**, 4318 (2001).
- [15] L. G. C. Rego and G. Kirczenow, *Phys. Rev. Lett.* **81**, 232 (1998).
- [16] T. Yamamoto, S. Watanabe, and K. Watanabe, *Phys. Rev. Lett.* **92**, 075502 (2004).
- [17] L. G. C. Rego and G. Kirczenow, *Phys. Rev. B* **59**, 13080 (1999).
- [18] O. Chiatti and et al., *Phys. Rev. Lett.* **97**, 056601 (2006).
- [19] K. Schwab, E. Henriksen, J. Worlock, and M. Roukes, *Nature* **404**, 974 (2000).
- [20] Y. Chalopin, J. N. Gillet, and S. Volz, *Phys. Rev. B* **77**, 233309 (2008).
- [21] R. Venkatesh, J. Amrit, Y. Chalopin, and S. Volz, *Phys. Rev. B* **83**, 115425 (2011).
- [22] L. Yang, N. Yang, and B. Li, *Nano Lett.* **14**, 1734 (2014).
- [23] M. Vaezi, H. Seitz, and S. Yang, *Int. J. Adv. Manuf. Technol.* **67**, 1721 (2013).
- [24] F. Lucklum and M. J. Vellekoop, *Procedia Engineering* **120**, 1095 (2015).
- [25] S. X. Yang, J. H. Page, Z. Y. Liu, M. L. Cowan, C. T. Chan, and P. Sheng, *Phys. Rev. Lett.* **93**, 024301 (2004).
- [26] S. X. Yang, J. H. Page, Z. Y. Liu, M. L. Cowan, C. T. Chan, and P. Sheng, *Phys. Rev. Lett.* **88**, 104301 (2002).
- [27] G. Chen, *Nanoscale Energy Transport and Conversion: A Parallel Treatment of Electrons, Molecules, Phonons, and Photons* (New York, Oxford University Press, 2005).
- [28] M. Büttiker, *Phys. Rev. Lett.* **57**, 1761 (1986).
- [29] R. Landauer, *IBM J. Res. Dev.* **1**, 223 (1957).
- [30] R. Landauer, *Phys. Lett. A* **85**, 91 (1981).
- [31] J. Ordonez-Miranda, L. Tranchant, S. Gluchko, and S. Volz, *Phys. Rev. B* **92**, 115409 (2015).
- [32] P. Ben-Abdallah, K. Joulain, J. Drevillon, and C. Le Goff, *Phys. Rev. B* **77**, 075417 (2008).
- [33] L. Lewin, *Polylogarithms and Associated Functions* (New York, Elsevier, 1981).
- [34] A. Alu and N. Engheta, *Phys. Rev. B* **74**, 205436 (2006).
- [35] E. D. Palik, *Handbook of Optical Constants of Solids* (Academic Press, Orlando, Florida, 1985).
- [36] W. G. Spitzer, D. A. Kleinman, and C. J. Frosch, *Phys. Rev.* **113**, 133 (1959).
- [37] Y. Chalopin, H. Dammak, M. Hayoun, M. Besbes, and J. J. Greffet, *Appl. Phys. Lett.* **100**, 241904 (2012).
- [38] K. Joulain, Y. Ezzahri, J. Drevillon, B. Rousseau, and D. DE Sousa Meneses, *Opt. Express* **23**, A1388 (2015).